Eggshell reinforced biocomposite—An advanced "green" alternative structural material

Boniface Jabik Tiimob, Shaik Jeelani, Vijaya Kumar Rangari

Department of Material Science and Engineering, Tuskegee University, 100 Chappie James Center, Tuskegee, Alabama 36088
Correspondence to: V. K. Rangari (E-mail: rangariv@mytu.tuskegee.edu)

ABSTRACT: The need for bio-based polymers as substitutes to recalcitrant petroleum sourced plastics is ever growing, because of increase in demand globally. Eggshell nanopowder (ENP) prepared using mechanical attrition and ultrasound irradiation was used to infuse a bio-based polymer [Super Sap 100/1000 epoxy (SSE)] for possible enhancement of its mechanical properties. The ENP, neat SSE and SSE/ENP composites were characterized using X-ray Diffraction, Transmission Electron Microscopy (TEM), Energy dispersive spectroscopy (EDS), Scanning Electron Microscopy, Thermogravimetic Analysis (TGA), Dynamic Mechanical Analysis (DMA), Thermomechanical Analysis (TMA) and flexure analysis. TEM and EDS analysis showed evidence of ENP in the SSE matrix whiles DMA and TMA analysis revealed significant improvements (7–22%) in the storage moduli and (3–17%) in coefficient of thermal expansion (CTE) respectively. Also, major delay in 5% decomposition temperatures and increases in char yields were observed in TGA analysis. The flexure strength, modulus, and toughness significantly improved by 6–31%, 11–37%, and 10–36%, respectively. Microstructure of fractured surfaces showed deflected crack paths which contributed to improve toughness. © 2015 Wiley Periodicals, Inc. J. Appl. Polym. Sci. **2016**, *133*, 43124.

INTRODUCTION

The organized interplay between organic and inorganic phases form materials with good mechanical performance. The mollusks shell which is mainly aragonite crystals carefully deposited on proteins has a well-defined structure and good integrity.[1] Hence, it is found to be extremely tougher than aragonite.[2] Emulating the design of natural composites is essential in structural engineering.[3] This can reveal new artificial structures with mechanical properties comparable to those of nature.[1] The chicken egg shell is another natural composite with emerging relevance. Millions of kilograms of waste chicken eggshells produced annually in the US pose a serious challenge to the environment.[4] The decomposing organic components leading to the emission of repugnant smell (H_2S) and the creation of an enabling environment for invasion by potential diseases causing pathogens as well as unattractive piles of residue are some of the issues with waste eggshells.[5] Alternative use of egg shell as components in structural materials will help in mitigating these challenges whiles providing for other societal needs. Few technologies are available for the processing of eggshells into useful products.[5,6] More innovations in recovery technologies for turning eggshells into resource materials are currently needed[7] to convert such natural and rich source of $CaCO_3$ into other forms that are useful for functional and sustainable material design.[8] Past findings show that the eggshell contains about 95% $CaCO_3$,[9] which can be used to modify the weak properties of polymers. The reinforcing effect of $CaCO_3$ has been studied with high-density polyethylene, nylon, polypropylene, polyketone, acrylonitrile butadiene styrene, and polyurethane. In these composites, the tensile and impact toughness significantly improved, because of the incorporation of the $CaCO_3$.[10] Hence, thermoplastic polymer reinforcement with $CaCO_3$ fillers has been well investigated but not much studies have been conducted with the filler in the current commercial bio-based thermosetting resins. Current research focus in green material design has intensified the use of bio-sourced fillers in biopolymer modification for enhancement of mechanical properties.[11–13] The Super Sap® 100/1000 epoxy (SSE) formulation currently has the highest plant-sourced renewable materials (~37%).[14] Unlike the petrochemical-based epoxies, it has superior properties such as excellent elongation, good adhesion, fast room temperature cure cycle, low sensitizing components for improved user safety, good wettability, and adhesion for the manufacturing of green composites. This formulation can significantly minimize the issues associated with climate change,

since it reduces CO and greenhouse gas emissions by a minimum of 50%,[14] the basis upon which it gained the United States Department of Agriculture (USDA) BioPreferred[SM] Product classification.[15] The problem however is that, the strength and stiffness of SSE are not good enough for advanced structural applications. Hence, our motivation is to work towards stepping-up these properties in SSE using Eggshell Nanopowder (ENP) as filler material. Attempts made so far, using natural fiber reinforcement in SSE composites yielded low mechanical properties, because of low fiber strength and weak interfacial bonding between the fibers and matrix.[16] In this work, the ENP is explored as an alternative reinforcement because of its sustainability and advantage of good compatibility with the SSE matrix. The inherent functionalization (hydroxyl, amine, and carboxylic groups) on ENP promotes hydrogen bonding with the matrix, unlike in artificially nucleated and rock sourced $CaCO_3$ which are not modified with any functional groups[17] Figure 1. Show the reaction of the monomeric units of the epoxy polymer with an amine hardener (cross-linking agent) and the possible interaction between the cross-linked polymer and functionalized ENP. It can be seen from this figure that hydrogen bond interactions between the electronegative elements of the ENP and those of the more electro positive unshielded hydrogens of the cross-linked polymer can very likely occur. Composites of ENP with the SSE formulations can therefore produce green and more biodegradable materials with significantly enhanced properties as attempted elsewhere using different reinforcement materials.[16,18]

MATERIALS AND METHODS

Materials

Egg shells were obtained from American Dehydrated Foods, Atlanta, GA and processed to separate crystal lumps from the egg proteins. These lumps were further processed into ENP using top-down techniques of nanomaterials synthesis. SSE resin was purchased from Entropy Resin. San Antonio, CA, and used to evaluate the reinforcing effects of the ENP. Polypropylene glycol (PPG) used as a liquid medium for the ball milling and denatured reagent grade ethanol (CH_3CH_2OH) used for washing the PPG and for ultra sonication were purchased from Sigma Aldrich, St. Louis, MO.

Preparation of the ENP

The eggshell is composed of layers of calcite deposited on collagen and glycosaminoglycons platforms. In order to release the calcite crystals, these organic platforms must be denatured. Hence the eggshells were boiled at 100°C in an electric cooker (Hamilton Beach, Model 33157) for 6 h, blended (Waring-Model 51BL30) at high speed for 10 min and thoroughly washed with H_2O in the initial stages and CH_3CH_2OH in the final stage before air drying at room temperature for 24 h. The ENP was prepared by ball milling 5 g of the microparticles in 10 mL of PPG with eight steel balls (6 mm) using Spex Sample prep 8000D mixer/mill for 10 h. This was then washed four times with absolute CH_3CH_2OH and centrifuged for 5 min at 15,000 rpm (Allegra 64R, Beckman Coulter). It was again mixed with 50 mL of CH_3CH_2OH and magnetically stirred at 1200 rpm for 30 min, then irradiated with ultrasound for 5 h
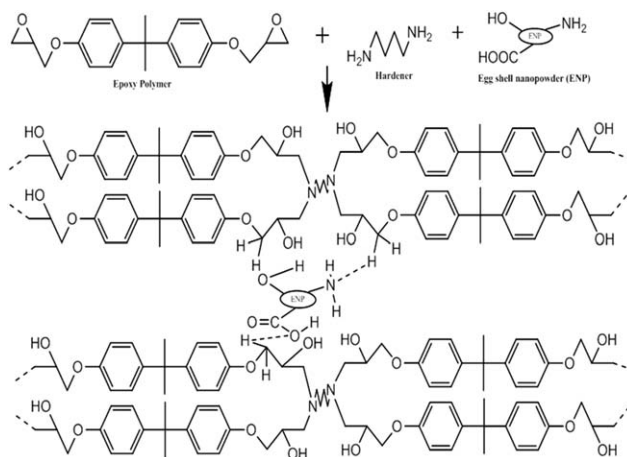

Figure 1. Mechanism of matrix interaction with ENP.

(Sonics vibra cell ultrasound, Model WCX 750, Ti-horn 20 kHz, 100 W/cm²) at 50% amplitude and 25°C. The ENP/CH_3CH_2OH suspension was then centrifuged at 15,000 rpm, and the ethanol decanted form the ENP. The ENP was then vacuum-dried for 24 h at room temperature.

Fabrication of SSE/ENP Nanocomposites

The ENP was infused in SSE resin in order to evaluate its effect on the thermal and mechanical properties of the SSE matrix. Specimens were prepared by mixing 2:1 ratios of part A and B of the resin for each of the distinct specimens. About 100 g of part A was first measured into a plastic beaker and 1, 2, 3, 4, 5, and 10 wt % ENP was categorically added and magnetically stirred at 1200 rpm for 12 h. This was then transferred into a 300 mL sample holder and 48 g of the part B (hardener) added, mixed and degassed consecutively for 3 min at 1200 and 1000 rpm in a Thinky mixer (ARE-250). These were then cast into standard silicone molds and left to cure at a controlled room temperature (25°C) for 24 h and then postcured at 48.8°C for 2 h in an oven (Isotem 200 series-230F). The specimens were allowed to cool to room temperature for 3 h before they were cut to standard sizes for Thermomechanical Analysis
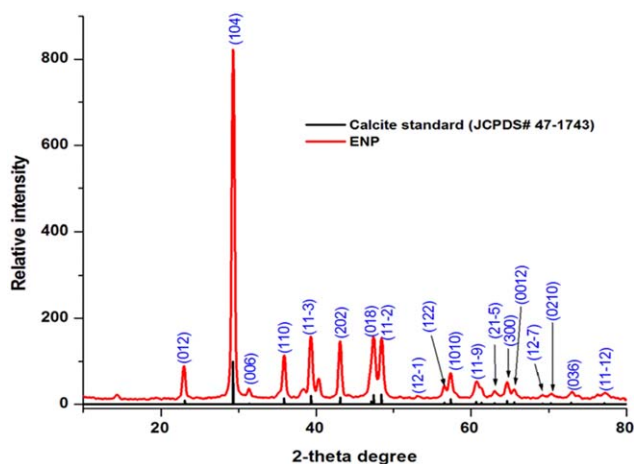

Figure 2. XRD patterns of eggshell nanoparticles. [Color figure can be viewed in the online issue, which is available at wileyonlinelibrary.com.]
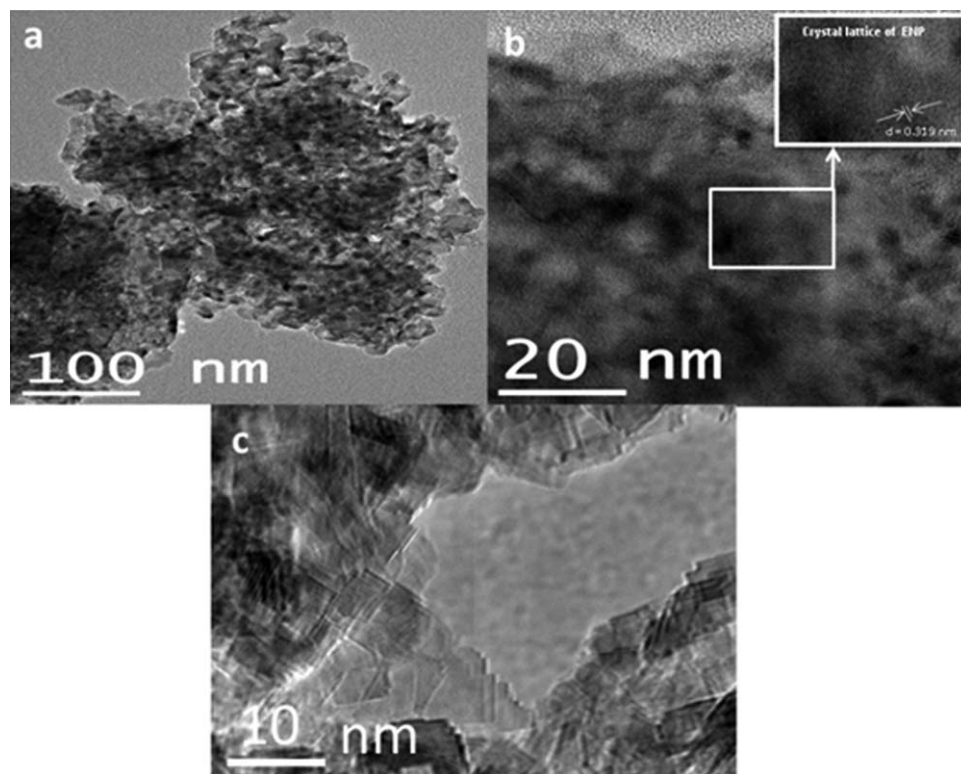
Figure 3. Transmission electron micrographs of the synthesized ENP: (a) Low; (b) Medium and (c) High magnification.

(TMA), DMA, Thermogravimetic Analysis (TGA), and flexure tests. At least seven (7) specimens were used in each of the thermal and mechanical tests.

X-ray Diffraction Analysis

X-ray Diffraction (XRD) pattern of the prepared ENP, the neat SSE and SSE/ENP nanocomposites were carried out using D-max 2100 X-ray diffractometer. This test was run at 40 kV and 30 mA, 5°/min sampling rate and width of 0.020 from 3° to 80° of 2θ angles.

Transmission Electron Microscopy

Transmission Electron Microscopy (TEM) analysis for the determination of particle sizes of ENP and its dispersion in SSE matrix were done using Joel 2010 microscope. One (1) mg of the ENP specimen was dispersed in 5 mL of ethanol for 10 min in an ultrasonic bath. A drop of the colloidal solution was deposited on a copper grid and used for the analysis. For the dispersion of ENP in the composite, 1 μL of each SSE/ENP composite liquid specimen was deposited on the copper grid and placed on a clean microscope slide to cure for 24 h before examination in the TEM.

Energy Dispersive Spectroscopy Analysis

Energy dispersive spectroscopy (EDS) which is coupled with the TEM was used to carry out elemental analysis on SSE/ENP nanocomposite specimens. The specimens were prepared as in the TEM analysis of SSE/ENP composites.

Dynamic Mechanical Analysis (DMA)

DMA was done using TA Q 800 equipment purge with N_2 gas at a flow rate of 50 mL/min. The equipment was set to operate at a frequency of 1 Hz, rate of 5°C/min from 30° to 150°C in a flexure mode. Specimens were cut to 60 $\times$ 12 $\times$ 3.5 mm as specified in ASTM standard D 4065-06[19] by rotor sanding under constant flowing tap water to avoid damage by heat build-up in the composite. The storage modulus and tan δ were analyzed using TA universal software.

Thermomechanical Analysis (TMA)

TMA was carried out to determine dimensional changes in the specimens, using TA Q 400 equipment in expansion mode.[20] CTEs were determined by using the ratio of change in dimension per unit dimension and change in temperature[21] and used to establish the dimension stability of each specimen. Specimens with 10 $\times$ 10 $\times$ 5 mm were subjected to constant probe force (0.2 N) in N_2 atmosphere (50 mL/min) and ramped at 5°C/min to 150°C. The CTEs (α) were determined in the ranges of (30–70°C) and (110–140°C) using TA universal software.

Thermogravimetic Analysis

TGA was performed using TA Q500 equipment to evaluate the thermal stability of the specimens. Approximately 12 mg of each specimen was analyzed in N_2 gas atmosphere (60 mL/min) by ramping at 10°C/min up to 600°C. The data were analyzed using TA universal software.

Flexure Analysis

Most epoxy-based composites are often used for structural applications. To help in the understanding of the behavior of such composites, flexure test which provides information on a material's response to three-point bend loading was evaluated. Flexure specimens with span-to-thickness ratio, l/d of 16, dimensions of 89 $\times$ 12.7 $\times$ 3.7 mm and span length of
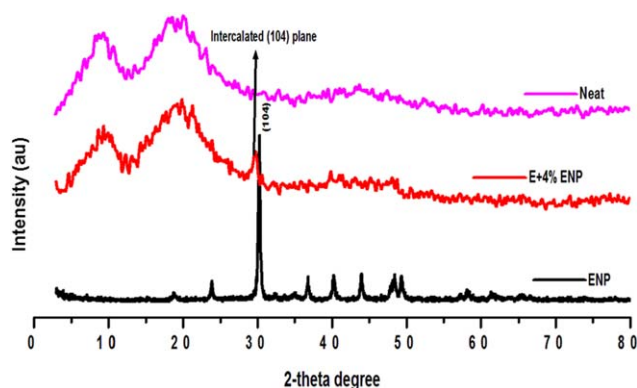
Figure 4. X-ray diffraction patterns comparing ENP, neat SSE, and SSE/ENP composite. [Color figure can be viewed in the online issue, which is available at wileyonlinelibrary.com.]

60 mm, in accordance to ASTM D790-10 test method B[21] was followed. Strain rate of 0.10 mm/min and a cross-head motion rate of 1.6 mm/min were used. This test was done on Zwick/Roell Z2.5 materials testing system equipped with TestXpert data acquisition system and a 2.5 kN load. The flexure strength, modulus and toughness were determined using the TextXpert software.

Scanning Electron Microscopy

Microstructural analysis of fractured surfaces of the tested specimens was done using JEOL JSM-5800 Scanning Electron Microscopy (SEM) operated at 10 kV. The specimens were coated with Au-Pd in Hummer 6.2 sputtering system purged with N_2 gas and operated at 20 militorrs, 5 volts and 15 mA for 5 min.

RESULTS AND DISCUSSION

Material Characterization

XRD and TEM Analysis. Figure 2 shows the X-ray diffraction pattern of the synthesized ENP and the standard from the data base. The nature of the diffraction peaks suggests that the inorganic phase is highly crystalline with crystal sizes in the nanometer range. TEM micrograph in Figure 3(a) shows that the particles are less than 100 nm (20–50 nm) in sizes, highly crystalline, irregular, and porous. The crystallinity can be clearly seen in the crystal lattice in Figure 3 b. The mapped region in Figure 3(b) shows the atomic arrangement of the crystals in a highly aligned pattern with a measured interplaner distance (d-spacing) of $\sim$ 0.319 nm. Figure 3(c) also shows an interesting arrangement of the crystal lattices of ENP in stacks of plate-like structures. This suggests that the ENP can adopt this type of arrangement to align in between polymer molecules, leading to enhancement in mechanical properties.

The X-ray diffraction patterns in Figure 4 are for ENP, neat SSE and SSE/4wt % ENP composite. The pattern for SSE/4wt % ENP composite clearly shows the existence of peak with crystal plane at (104) because of the ENP reinforcement in the composites. SSE is observed to intercalate the crystal lattice of ENP by the shift in diffraction angle, $2\theta = 30.24°$ of (104) plane to $2\theta = 29.68°$ in the nanocomposites. This corresponds to a shift in inter-planer distance, d (104) = 0.295 nm of the ENP to d (104) = 0.301 nm of SSE/4 wt % ENP, calculated using Bragg's equation[13]:

$$d_{hkl} = \frac{\lambda}{2\sin\left(\frac{\pi\theta}{180}\right)} \quad (1)$$

where λ is the wavelength of CuKα radiation (1.54 Å) and θ is the angle of diffraction. This implies that the plate-like structure of ENP observed in Figure 3(c) is most likely maintained in between the polymer molecules in the composite. Similar results have been observed in polyethylene oxide intercalated graphite oxide.[22]

The TEM images of SSE/4 wt % ENP composite low and high magnifications are shown in Figure 5(a,b) respectively. The dark and irregular shaped ENP are revealed to be well dispersed in the SSE matrix. This good dispersion provides more sites for better
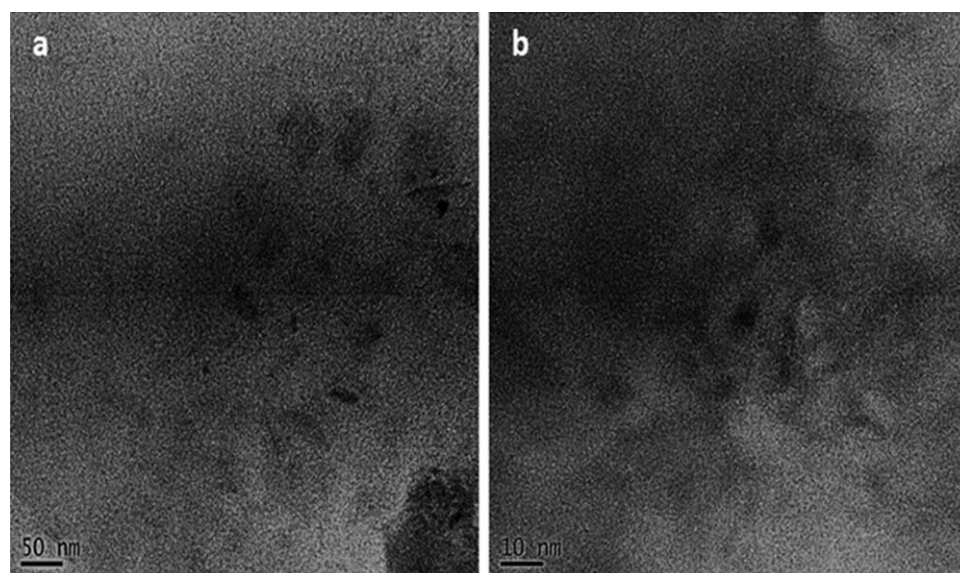

Figure 5. TEM images: (a) low and (b) high magnification of 4 wt % ENP dispersed in SSE.

Table I. Effect of ENP on the Thermal Stability of SSE System

| Specimen | Onset of decomposition | Decomposition temperatures (°C) | | Residual yield at 550°C % |
		@ 5 wt %	@ 50 wt %	
Neat	327.54 ± 2.11	186.20 ± 5.80	375.80 ± 0.85	3.73 ± 0.47
E+1 wt % ENP	315.71 ± 1.01	193.19 ± 2.42	365.55 ± 0.49	5.34 ± 0.83
E+2 wt % ENP	321.03± 0.62	219.21 ± 8.62	368.95 ± 0.50	8.45 ± 0.11
E+3 wt % ENP	320.57 ± 0.84	159.70 ± 2.32	370.00 ± 0.57	6.82 ± 0.51
E+4 wt % ENP	321.99 ± 1.36	205.68 ± 1.92	366.26 ± 0.48	9.69 ± 0.79
E+5 wt % ENP	264.01 ± 1.90	160.22± 13.01	305.03 ± 1.32	15.02 ± 0.33
E+10wt % ENP	265.22 ± 2.11	157.03± 11.75	304.22 ± 0.65	18.10± 0.49

ENP-SSE interfacial interaction and considerably enhances the strength and modulus of the composite through a better stress transfer mechanism. However, 5 and 10 wt.% loading led to decrease in mechanical properties, because of reduced interparticle distances between highly concentrated ENP particles which have high affinity for one another and turn to exist in agglomerated clusters. It has been shown elsewhere[13] that the dispersion of 3 wt % ENP in soy protein isolate is better than those of 5 and 10 wt %, leading to more improvement in tensile strength and young's modulus through an efficient stress transfer mechanism. In another study, TEM analysis revealed that good dispersion of 2 wt % bio-$CaCO_3$ in the matrix of bioplast GS 2189 led to high flexure strength.[11] This means that good dispersion contributes immensely to the enhancement of mechanical properties of composite as affirmed in the findings with ENP/SSE composites in this article.

Thermogravimetric Analysis. The addition of $CaCO_3$ NPs contributed to delays in the thermal degradation at the early stages of the decomposition for 1–4 wt. ENP and increment in residual yield. Table I shows that the temperatures at 5% weight loss increases for the composites, except for 3%, 5%, and 10% loading of $CaCO_3$. Onset temperature and 50% decomposition temperatures of the composites reduced from those of the neat SSE system. The increase in residue can be attributed the remnants of the inorganic particles and char, formed during the degradation to slow down the combustion of the polymer. Char is also responsible for the impermeability of volatile components which accelerates combustion.[23–26] ENP is porous in nature,[17,27] hence, it can permit the infiltrations of volatile components to accelerate thermal decomposition. However, delays in 5% decomposition is due blockage of the pores by early stage char formation. With increase in temperature, ENP expand and open the pores to facilitate the diffusion of volatiles and combustion. Leading to decrease in 50% decomposition temperatures of all the composites. It is worthy to mention that at 5 and 10 wt % loading of ENP, the decomposition temperatures fell below those of the neat. This property deterioration which is also realized in mechanical properties for these composites can be attributed to poor dispersion, leading to less particle to matrix interaction from agglomerated ENP at higher concentrations. High loading of $CaCO_3$ has been found to have led to reduction in thermal stability of soy protein isolate and bioplast GS 2189 resins[11,13]

as observed in this work for ENP/SSE nanocomposites with high content of ENP. The thermal decomposition temperatures at higher concentrations do show some randomness, this is probably due to agglomeration effects. Uneven distribution of ENP in SSE matrix can lead to the analysis of specimens which either contain less or more ENP nanoparticles, especially in this case where ~12 mg amount of each specimen was used.

This finding supports a report, which showed that an increasing amount of $CaCO_3$ NPs led to lower thermal degradation temperature in poly (lactic acid).[28] However, another report showed improvement in thermal stability with bioplast GS 2189.[11] The increase in residue is because of the presence of proportionate amount of CaO from the transformation of ENP in the composites at higher temperature and char from the matrix which contributed to retard thermal degradation.[27]

Dynamic Mechanical Analysis. The dynamic mechanical analysis of viscoelastic properties of the specimen showed that, at temperatures below 65°C, the storage moduli for all the composites considerably improved by 149–457 MPa (7–22%) over that of the neat epoxy system as the amount of ENP is increased from 1, 2, 3, 4, 5, and 10 wt %. Figure 6 reveals that maximum
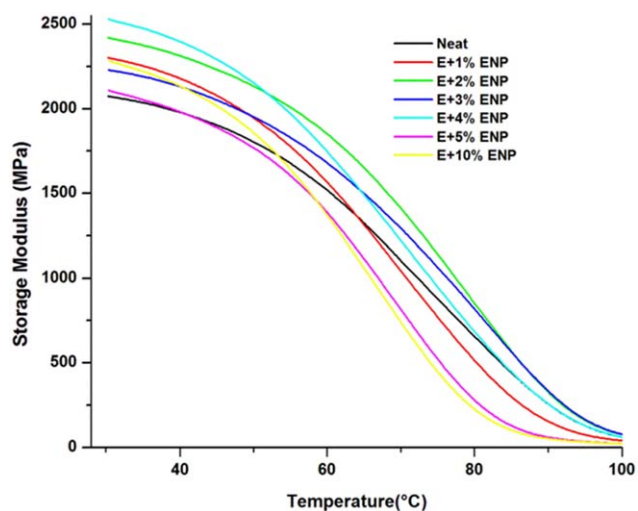

Figure 6. Storage moduli of neat and SSE/ENP systems. [Color figure can be viewed in the online issue, which is available at wileyonlinelibrary.com.]

Table II. Storage Modulus of SSE/ENP Nanocomposites

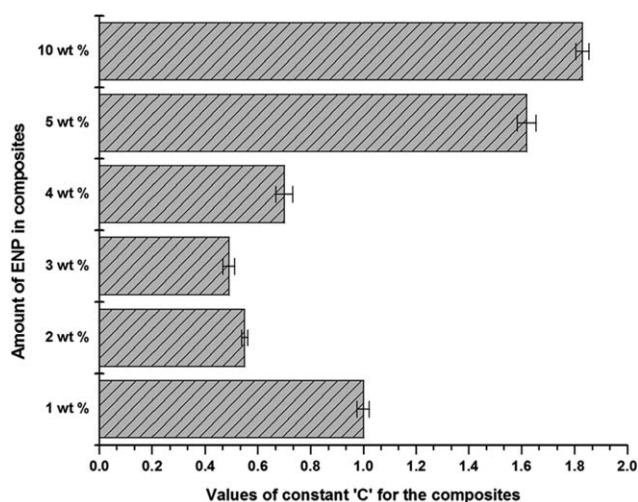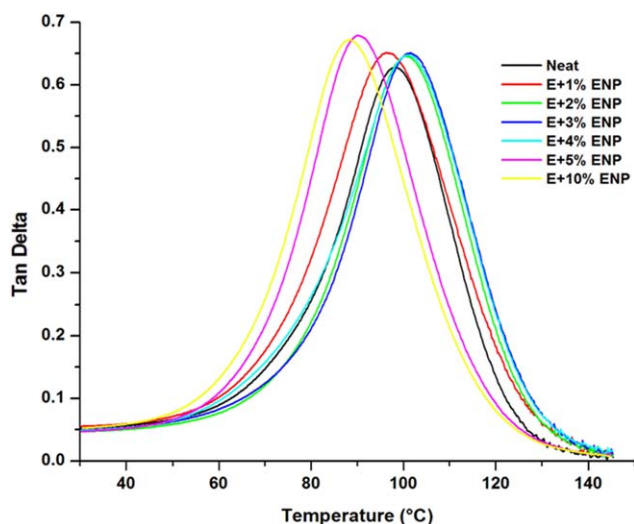| Specimen	Storage modulus (MPa)	
	@ 30°C	@ 100°C
Neat	2075.32 ± 21.05	35.12 ± 0.52
E+ 1 wt % ENP	2301.22 ± 47.35	39.30 ± 0.99
E+ 2 wt % ENP	2484.02 ± 89.32	76.13 ± 0.25
E+ 3 wt % ENP	2229.30 ± 80.22	76.21 ± 0.86
E+ 4 wt % ENP	2531.23 ± 38.09	61.08 ± 0.23
E+ 5 wt % ENP	2110.15 ± 26.01	22.41 ± 0.39
E+ 10 wt % ENP	2282.35 ± 34.25	21.33 ± 0.44

improvement was realized in 4 wt % loading of ENP and suggests more ability to store elastic energy over the other specimens. It has been shown that high exfoliation of CaCO₃ NPs led to improvement in the storage of elastic energy by bioplast[11] GS 2189 whiles with poly (lactic acid) good dispersion and strong interfacial interactions led to enhancements in both storage modulus and Tg.[28]

The effectiveness of the filler on the modulus of the nanocomposites can be determined by calculating the value of constant C from eq. (2) as in Kumar et al.[28]

$$C = \left(E'_g / E'_r \right) \text{composite} / \left(E'_g / E'_r \right) \text{resin} \qquad (2)$$

E'_g and E'_r represent the storage modulus at glassy and rubbery regions, respectively. Lower values of C indicates more effectiveness of the filler. In this work the storage moduli at 30°C and 100°C in Table II for glassy and respective rubbery regions were used to determine the effectiveness of the ENP on the modulus of the matrix using eq. (2).

High value of the constant C is found to occur in 1, 4, 5, and 10 wt % loading of ENP whereas low values occurred in 2 and 3 wt % as shown in Figure 7. This implies that the effectiveness of ENP in enhancing the storage modulus of SSE is more at 2 and 3 wt % concentrations. This reflects in the flexure modulus

Figure 8. Tan δ curve of SSE resin system infused with ENP. [Color figure can be viewed in the online issue, which is available at wileyonlinelibrary.com.]

and strength of 3 wt % ENP composite which revealed the highest improvement in mechanical properties.

The Tg for the SSE/ENP nanocomposites obtained from the peak of the tan δ curves showed an increase of 2–3°C in 2, 3, and 4 wt % ENP loaded composites, but 1, 5, and 10 wt % loading revealed a reduction as shown in Figure 8. Similar increase in Tg from the peak of the tan δ curve of bio-CaCO₃/ GS 2189 bioplast nanocomposite has been reported.[11] This improvement in damping properties of composites with CaCO₃ is an affirmation of its reinforcing effects.

Thermomechanical Analysis. The inclusion of ENP led to improvement in dimensional stability of the epoxy resin. A reduction in the coefficient of thermal (CTE) expansion by a minimum of 9% (2 wt % loading) and a maximum of 17% (because of 4 wt. % loading) from that of the neat specimen before the glass transition region is significant, with such low amount of reinforcement. It is desirable to obtain more improvement with small

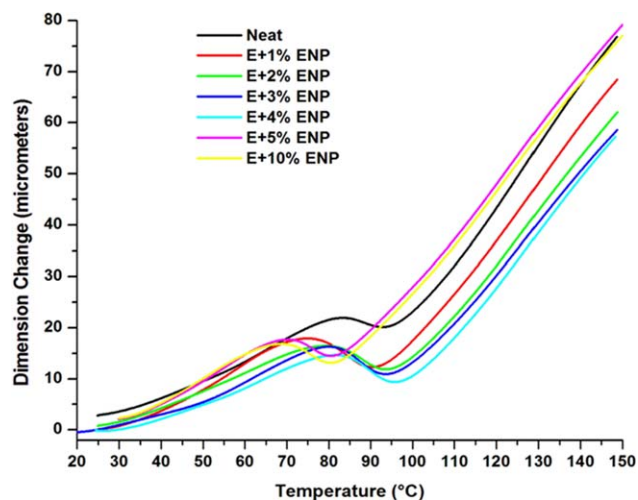**Figure 7.** Effectiveness of ENP on the storage modulus of SSE resin.

Figure 9. Dimensional stability of SSE/ENP nanocomposites. [Color figure can be viewed in the online issue, which is available at wileyonlinelibrary.com.]

Table III. Changes in CTEs of SSE/ENP Nanocomposites

Specimen	CTE [α-μm/(m. °C)]		Change in CTE [%]	
	Before Tg [30–70°C]	After Tg [110–140°C]	Before Tg	After Tg
Neat	81.14 ± 3.14	241.28 ± 2.81	–	–
E+ 1 wt % ENP	88.48 ± 0.25	218.53 ± 6.98	−9.04 ± 0.12	9.43 ± 0.13
E + 2 wt.% ENP	73.94 ± 0.86	230.11 ± 1.12	8.87 ± 0.17	4.63 ± 0.15
E + 3 wt % ENP	73.31 ± 1.35	231.53 ± 2.25	9.65 ± 0.20	4.04 ± 0.22
E + 4 wt % ENP	67.55 ± 0.09	234.65 ± 1.03	16.74 ± 0.23	2.74 ± 0.30
E + 5 wt % ENP	86.89 ± 10.09	224.36± 5.85	−7.09 ± 0.13	7.01 ± 0.09
E + 10 wt % ENP	86.57 ± 1.12	226.16 ± 6.05	−6.69 ± 0.16	6.27 ± 0.11

amount of nanomaterial because higher concentrations tend to compromise the mechanical properties of the matrix as observed in 5 and 10 wt % ENP loadings. This is evident in the reduced dimension stability before the Tg region and the lowering of the Tg of their composite systems in Figure 9. Figure 9 also shows that before Tg, the slopes of the straight line regions of the composites are lower than that of the neat specimen, except for 1, 5, and 10 wt % ENP loadings. These indicate improved dimension stability. The CTEs after the Tg region also ranged from 3% to 9% reduction

over that of the neat as shown in Table III. Similar results have been reported in CaSiO$_3$/SSE nanocomposites.[12] Also, a study of CaCO$_3$/bioplast showed improved dimension stability[11] because of stiffer and deformation resistant CaCO$_3$ NPs which tend to restrict the motion of chain segments of the polymer.[29]

Flexure Test. The flexure strength, modulus, and toughness of the neat system were 70.21± 1.62 MPa, 1.96 ± 0.06 GPa, and 4178.30 ± 67.50 Jm^{-3} respectively. The incorporation of ENP (1,
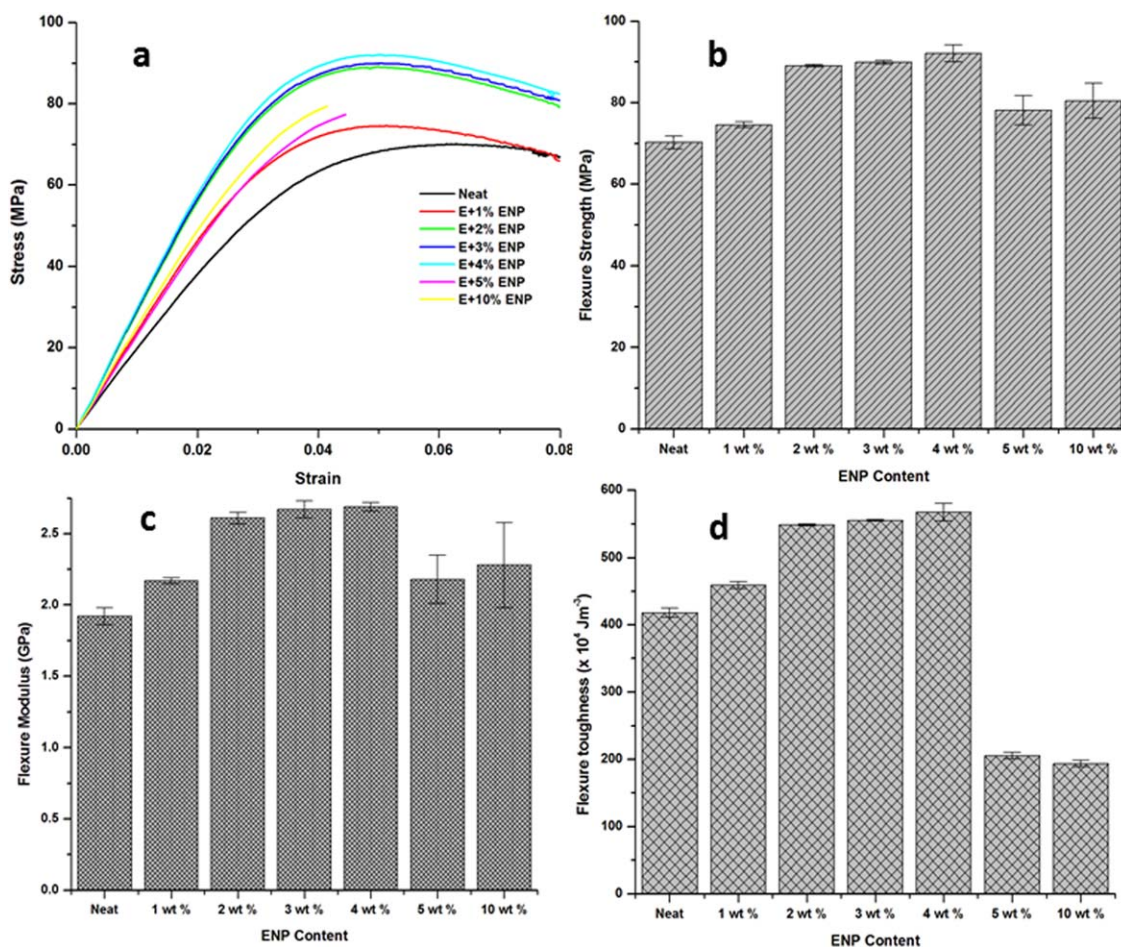

Figure 10. Effect of ENP on flexure properties of epoxy specimen: (a) Stress–strain curves of SSE/ENP composites; (b) flexure strength; (c) flexure modulus, and (d) flexure toughness. [Color figure can be viewed in the online issue, which is available at wileyonlinelibrary.com.]
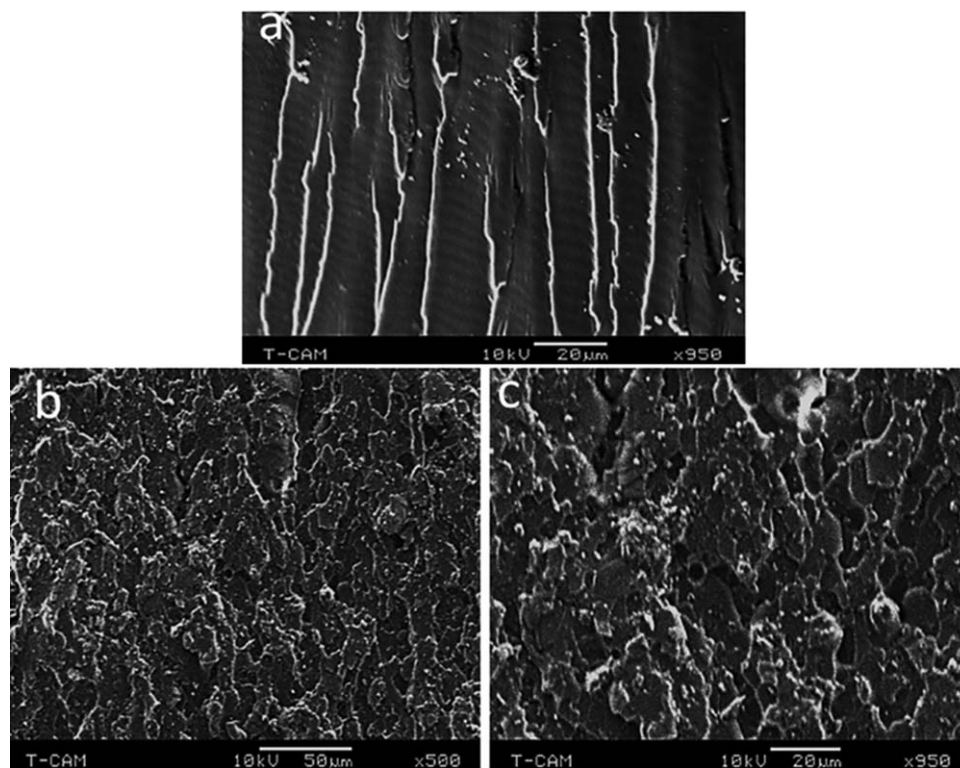
Figure 11. Microstructure of fractured surfaces for (a) neat and (b-c) SSE/4 wt % ENP nanocomposite.

2, 3, 4, 5, and 10 wt %) correspondingly led to increase in flexure strength, modulus, and toughness as shown in Figure 10(a–d). The improvement in flexure strength ranged from 6.20–31.15% for 1–10 wt % loading of ENP. Also the enhancements in modulus and toughness ranged from 10.71–37.24% and 10–36% respectively. Flexure toughness were obtained from the integral areas under the stress–strain curves using Origin version 6.0 software. The results show that 5 and 10 wt % ENP loading had less influence in dictating the level of enhancement in strength and modulus as compared to 2–4 wt % loading of ENP. This is because of poor dispersion (agglomerations) and weak interfacial interactions between SSE molecules and ENP at higher concentrations of ENP. However, considerable improvement in the mechanical properties at 3–4 wt % ENP can be attributed to good filler to polymer interfacial interactions and good dispersion. Also, the porous and irregular morphologies of ENP can facilitate the attachment of the polymer matrix onto the particles in a manner that favor particle to polymer interaction. Moreover, amine, carboxylic, and hydroxyl functional groups in the egg shell remain in ENP after the processing of the eggshell[17] and can enhance the interaction between ENP and SSE through hydrogen bonding as shown in the mechanism in figure 1. Modified $CaCO_3$ with silane coupling agent (KH550) has been found to have led to improvement in strength and toughness in epoxy/fiber composite.[30] Also, about 13.5%, 6.1%, 42.5%, and 106.3% improvements in strength, modulus, displacement, and total fracture work was respectively obtained by unmodified nano-$CaCO_3$.[29] Furthermore, nanosized $CaCO_3$/polylactide nanocomposites showed improvement in strain-at-break over a pure polylactide system[10] whereas, a study on fracture toughness and deformation mechanism of polypropylene/$CaCO_3$ composites

showed that the addition of 15 wt % $CaCO_3$ NPs led to increase in the fracture toughness by 180%.[31] Also, polypropylene/polyolefin elastomer (PP/POE)/nano-$CaCO_3$ ternary composites[32] showed significant increase in notched impact toughness over PP/POE blend and neat PP. Again, the use of chemical foaming agents to incorporate $CaCO_3$ into poly (propylene carbonate) produced completely biodegradable foam composite with enhanced compressive strength associated with well-developed cell morphology[33] whiles bio-based nanocomposites fabricated by infusion of $CaCO_3$ nanoparticles into Polylite® 31325-00 resin led to significant improvement in compressive strength (14%) and modulus (27%) in 2% bio-$CaCO_3$/Polylite 31325 nanocomposite against the neat system.[34] Another study on poly (ε-caprolactone) (PCL)-coated microsized $CaCO_3$ and noncoated $CaCO_3$ melt blended with Polylactide (PLA) revealed that toughness of the composites is immensely improved by the incorporation of PCL-coated $CaCO_3$ microparticles; whereas the elongation at break improved by 310%.[35] Furthermore, when poly (L-lactide) (PLA) was melt-mixed with micro and nanosized $CaCO_3$ particles before and after modification with calcium stearate, it showed considerable improvement in tensile strength and modulus with less compromise in the elongation at break because of the inclusion of nanosized $CaCO_3$ by up to 30 wt %.[36] Regardless of the emphasis laid on the improvement in mechanical properties by the aforementioned investigations, another study revealed that nano-$CaCO_3$ dispersed in polystyrene matrix led to reduction in tensile strength and toughness from that of neat polystyrene; because of surface defect-induced interfacial debonding and filler agglomerations.[37] The findings about mechanical property improvement with ENP/SSE nanocomposites support these reports.
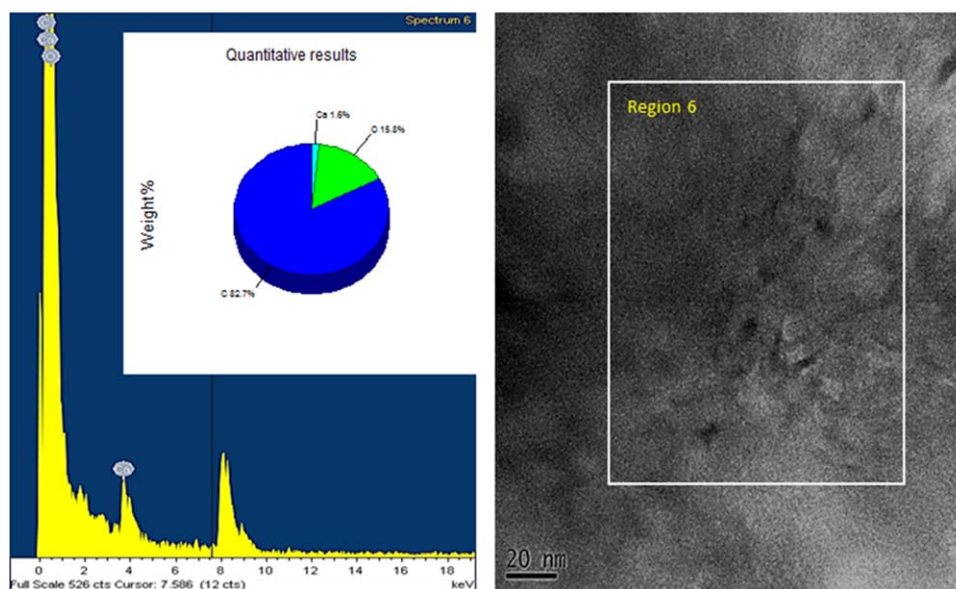
Figure 12. EDS elemental analysis of the mapped region on SSE/4 wt % ENP nanocomposite. [Color figure can be viewed in the online issue, which is available at wileyonlinelibrary.com.]

SEM Microstructural Analysis. The fractured surfaces were probed using a scanning electron microscope. The micrographs in Figure 11(a–c) show the fractured surface of the neat SSE and those of SSE/4% wt. ENP after flexure test. The fractured surface for the neat [Figure 11(a)] specimen show uninterrupted crack paths propagated along the thickness direction. The pallets on isolated portions are pieces of the polymer matrix which cracked partially, but are loosely bound to the fractured surface. The nature of this surface suggests a brittle failure, because the surface is smooth whiles the cracks are propagated uninterruptedly. However, the microstructures of the nanocomposite show rough ridge-like patterns and river markings [Figure 11(b,c)]. These are indications of crack path deflection and ductility adopted by the composite in the presence of ENP. The cracks are deflected around these shapes to delay, failure in the SSE/ENP composite. Similar microstructure, thermal and mechanical properties have been reported elsewhere for $CaSiO_3$/SSE nanocomposites.[12] This could be because of the similar group chemistry by carbon and silicon which are the distinguishing elements in both reinforcement materials ($CaSiO_3$ and $CaCO_3$). Figure 11(b,c) also shows evidence of microvoids in the composites. These flaws serve as stress concentration points in the materials and immensely lead to compromises in mechanical properties and unexpected failures.[29] This indicates that there is high potential for further improvement in mechanical properties if the flaws can be minimized.

Energy Dispersive Spectroscopy. ENP on the fractured surface is not visible by the SEM, since it is limited in capacity to detect nanoscale materials. However, the evidence of ENP in the composite was analyzed by XRD (Figure 3), TEM (Figure 5), and EDS shown in Figure 12. The micrograph and pie chart (Figure 12) show the elemental composition and the amount of each element in the mapped region 6 on the SSE/4 wt % ENP nanocomposite. The evidence of 1.6% Ca is exclusively due to ENP whiles 15.8% O and 82.7% C are because of contributions

from both SSE and ENP. This indicates that ENP is embedded in the SSE molecules in the composites. In a different study, EDS analysis of ENP/soy protein isolate composites revealed the presence of Ca as evidence for the existence of ENP in the polymer matrix.[13] This is in agreement with the EDS results for ENP/SSE composites.

CONCLUSIONS

Eggshell nanopowder (ENP) was synthesized, characterized, and used as filler in a bio-based epoxy formulation to fabricate nanocomposites. XRD results of the composite specimen showed an intercalated morphology of the composites because of the inclusion of ENP particles. TEM and EDS analysis confirmed the existence of ENP in the SSE Matrix. TGA showed significant delays in 5% decomposition temperatures and proportionate increases in residual yields because of the addition of ENP. Dynamic mechanical analysis, thermomechanical, and flexure analysis also respectively revealed significant improvement in storage moduli, dimension stability, flexure strength, modulus, and toughness because of the incorporation of 2–4 wt % ENP. These suggest that ENP is highly reinforcing and can be used for the enhancement of polymer structures. SEM probe of fractured surfaces of SSE/ENP composites revealed rough microstructure different from the uninterrupted crack paths evident on the surface of the pure SSE system, suggesting that ENP interacted with the matrix in such a manner that led to the deflection of the cracks to delay catastrophic failures which otherwise could abruptly occur as observed in the neat SSE system. Therefore, improvements in mechanical properties are because of the ENP acting as crack arresters. In effect, ENP is highly reinforcing, cheap, and can serve as sustainable and alternative natural filler to the SSE matrix and other biopolymers in the manufacture of green materials with high structural integrity.

REFERENCES

1. Katti, K. S.; Mohanty, B.; Katti, D. R. *J. Mater. Res.* **2006**, *21*, 1237.

2. Olderøy, ØM.; Xie., M.; Strand, L. B.; Flaten, E. M.; Sikorski, P. A. *Cryst. Growth. Des.* **2009**, *9*, 5176.

3. Jia, X.; Kiick, L. K. *Macromol. Biosci.* **2009**, *9*, 140.

4. Walton, H. V.; Cotteril, O. J.; Vandepop, J. M. *Poult. Sci.* **1973**, *52*, 1836.

5. Felipe-Sese, M.; Eliche-Quesada, D.; Corpas-Iglesias, A. F. *Ceram. Int.* **2011**, *37*, 3019.

6. R. G. Adams, M. R. Franklin, U.S. Patent 7017, 277 B1. **2006**.

7. Dodson, R. J.; Hunt, J. A.; Parker, L. H.; Yang, Y.; Clark, H. *J. Chem. Eng. Process.* **2012**, *51*, 69.

8. Tiimob, B.; Apalangya, V.; Samuel, T.; Jeelani, S.; Rangari, V. *Brit. J. Appl. Sci. Technol.* **2015**, *8*, 180.

9. Nys, Y.; Gautron, J.; Garcia-Ruiz, M. J.; Hincke, T. M. C. *R. Palevol.* **2004**, *3*, 549.

10. Jian, L.; Zhang, J.; Wolcott, M. P. *Polym.* **2007**, *26*, 7632.

11. Hassan, A. T.; Rangari, K. V.; Jeelani, S. *ACS Sustain. Chem. Eng.* **2014**, *2*, 706.

12. Tiimob, J. B.; Rangari, K. V.; Jeelani, S. *J. Appl. Polym. Sci.* **2014**, *131*, 40867.

13. Rahman, M. M.; Netravali, N. A.; Tiimob, J. B.; Rangari, K. V. *ACS Sustainable Chem. Eng.* **2014**, *2*, 2329.

14. Entropy Super Sap 100/1000. http://www.entropyresins.com/sites/default/files/SuperSap-100_1000_TDS.pdf (Accessed April 25, **2015**).

15. ASTM Standards, D6866-11.*ASTM International* **2011**,

16. Masoodi, R.; El-Hajjar, F. R.; Pillai, M. K.; Sabo, R. *Mater. Des.* **2012**, *36*, 570.

17. Apalangya, V.; Rangari, V.; Tiimob, B.; Jeelani, S.; Samuel, T. *Appl. Surf. Sci.* **2014**, *295*, 108.

18. Wang, S.; Masoodi, R.; Brady, J.; George, R. B. *J. Renew. Mater.* **2013**, *1*, 279.

19. Wypych, G. Handbook of Fillers-A Definitive User's Guide and Databook; ChemTec Publishing: Toronto, **2000**.

20. Ma, M.; Zhu, J.; Sun, R.; Chen, F.; Zhu, Y. *Mater. Lett.* **2011**, *65*, 424.

21. Li, S.; Jia, N.; Zhu, J.; Ma, M.; Sun, R. *Carbohydr. Polym.* **2010**, *80*, 270.

22. Salto, F.; Guomin, M.; Hanada, M. *Solid State Ionics* **1997**, *101*. 37.

23. Liu, T.; Tjiu, C. W.; He, C.; Na, S. S.; Chung., S. T. *Polym. Int.* **2004**, *53*, 392.

24. Corcione, E. C.; Frigione, M. *Mater.* **2012**, *5*, 2960.

25. Krump, H.; Luyt, A. S.; Hudec, I. *Mater. Lett.* **2006**, *60*, 2877.

26. Liang, Z. M.; Yin, J.; Wu, J. H.; Qiu, Z. X.; He, F. F. *Eur. Polym. J.* **2004**, *40*, 307.

27. Hassan, A. T.; Rangari, K. V.; Rana, K. R.; Jeelani, S. *Ultrason. Sonochem.* **2013**, *20*, 1308.

28. Kumar, K.; Dev, A.; Gupta, P. A. *Composites Part B* **2014**, *56*, 184.

29. Asif, A.; Rao, V. L.; Saseendran, V.; Ninan, K. N. *Polym. Eng. Sci.* **2009**, *49*, 756.

30. He, H.; Zhang, Z.; Wang, J.; Li, K. *Composites Part B* **2013**, *45*, 919.

31. Afshar, A.; Massoumi, I.; Khosh, R. S.; Bagheri, R. *Mater. Des.* **2010**, *31*, 802.

32. Ma, G. C.; Mai, L. Y.; Rong, Z. M.; Ruan, H. W.; Zhang, Q. M. *Compos. Sci. Technol.* **2007**, *67*, 2997.

33. Jiao, J.; Xiao, M.; Shu, D.; Li, L.; Meng, Y. Z. *J. Appl. Polym. Sci.* **2006**, *102*, 5240.

34. Hassan, A. T.; Rangari, K. V.; Jeelani, S. *J. Appl. Polym. Sci.* **2013**, *130*, 1097.

35. Zhang, Y.; Meng, B.; Chen, L.; Tao, J.; Wu, Z. *J. Appl. Polym. Sci.* **2012**, *125*, 952.

36. Kim, H.-S.; Park, B. H.; Choi, J. H.; Yoon, J.-S. *J. Appl. Polym. Sci.* **2008**, *109*, 3087.

37. Gao, Y.; Liu, L.; Zhang, Z. *Acta Mech. Sodica. Sin.* **2009**, *22*, 555.